A stratigraphically controlled multi-proxy chronostratigraphy for the Eastern Mediterranean

Casford[1] J.S.L., R. Abu-Zied[2], E.J. Rohling[3], S. Cooke[4], C. Fontanier[5], M. Leng[6], A. Millard[7] and J. Thomson[2]

[1] Department of Geography, Durham University, Science site, Durham DH1 3LE, UK.

[2] Geology Department, Mansoura University, El-Mansoura: 35516, Egypt

[3]National Oceanography Centre, European Way, Southampton, SO14 3ZH, UK.

[4]Department of Earth & Ocean Sciences, University of Waikato, Hamilton, New Zealand

[5]Laboratoire des Bio-Indicateurs Actuels et fossils, UFR Sciences, 49045 Angers, France

[6] School of Geography, University of Nottingham, Nottingham, NG7 2RD, UK.

[7]Depatment of Archaeology, Durham University, Science site, Durham DH1 3LE, UK.

Abstract

An AMS ^{14}C dated multi-parameter event stratigraphy is developed for the Aegean Sea based on highly resolved (centimetre to sub-centimetre) multi-proxy data collected from four Late Glacial to Holocene sediment cores. We quantify the degree of proportionality and synchroneity of sediment accumulation in these cores and use this framework to optimise the confidence levels in regional marine, radiocarbon-based chronostratigraphies. The applicability of the framework to published, lower resolution records from the Aegean Sea is assessed. Next this is extended into the wider Eastern Mediterranean, using new and previously published high-resolution data from the Northern Levantine and Adriatic cores. We determine that the magnitude of uncertainties in the intercore comparison of AMS ^{14}C datings based on planktonic foraminifera in the Eastern Mediterranean is of the order of ± 240 years (2SE). These uncertainties are attributed to syn- and post- sedimentary processes that affect the materials dated. This study also offers a background age-control that allows for vital refinements to radiocarbon-based chronostratigraphy in the Eastern Mediterranean, with the potential for similar frameworks to be developed for any other well-studied region.

Introduction and rationale

The Aegean and Mediterranean Seas are of particular importance to palaeoceanography, as the limited volumes of these basins promote rapid responses to climatic change. Due to the restricted communication with the open ocean, these responses are also amplified in comparison with oceanic signals. Together with the enhanced sediment accumulation rate common in marginal basins, this allows detailed records of change to be preserved, and facilitates high-resolution sampling [Bethoux et al., 1999]. However, to interpret this wealth of information accurately, good dating constraints are essential [Sarnthein et al., 2000].

Unfortunately, high accumulation rates commonly increase the probability of sediment reworking. It has been suggested that much of the sediment in the Mediterranean is re-deposited, with some estimates ranging as high as 75% [Stanley, 1985]. Another pervasive problem in marine cores is bioturbation, which mixes older and more recent material. Hence, individual AMS dating results are not as reproducible as one would wish. Careful sample selection can increase the accuracy of individual datings, but even small amounts of allochthonous 'old' carbon, normally impossible to detect when picking material, may cause significant anomalies, biasing results toward older ages. For example a 10% increase in 'dead' carbon in a sample will result in an age biasing of ~800 radiocarbon convention years.

Jorissen et al. [1993] reported wide dating ranges for the timing of I/II and II/III biozonal boundaries in the Mediterranean, spanning 950 and 1270 years, respectively. The association of these boundaries with the global glacial Terminations 1a and 1b in their records suggests that the dating range is not real, but a likely artefact due to dating uncertainties. Jorissen et al. [1993] also note offsets in the radiocarbon ages for a number of evident lithological horizons between Adriatic cores IN68-9 and IN68-5 (only 100 km apart), with offsets non-systematically varying between 300 and 1400 years, suggesting dating uncertainties. Moreover sequences of dating within a single core may also highlight uncertainties. For example, Jorissen et al. [1993] show several instances of dating “reversals” within individual cores. Similarly core KET 8216 from the Adriatic shows an 800-year difference between virtually adjacent datings from below and above the base of the sapropel (S1) [Fontugne et al., 1989]. These datings are only 3 cm apart and the suggested separation would require an almost 3-fold reduction in the average sedimentation rate of the core. Although individual datings may be offset from “true” age by variation in the reservoir age, this is unlikely to explain substantial dating reversals or large age differences between narrowly spaced samples. These offsets are more likely to have resulted from sedimentary processes affecting the material that was dated.

The main sedimentary processes concerned involve remobilization and redeposition of previously deposited materials and/or bioturbational mixing. Bioturbation effects have been previously discussed, in general [Bard 2001] and for the specific example of *Zoophycos* burrows [Löwemark and Werner 2001, Bromley and Hanken 2003]. Löwemark and Werner [2001] emphasise that there can be considerable difficulty in recognising *Zoophycos* traces in unconsolidated sediments, and suggest that such burrows may cause age falsifications of as much as 1110-2525 years. These effects are not limited to the remobilization of older material by burrowing, but may also include the pushing of younger material down into older sediments by up to 1m.

Thus the real limitations to age accuracy are not instrumental but, determined by the nature of the dated materials and the sedimentary history. Datings on a single horizon are best viewed as individual samples from a probability function, which we aim to quantify here. The distribution of dates in previous work (see above) suggests that in the Eastern Mediterranean as a whole, margins of "error" might be expected in the order of ± 800 years.

Our high-resolution Aegean records provide a unique opportunity to constrain a regional Aegean chronostratigraphic framework, by comparing and contrasting detailed multi-proxy stratigraphic and AMS ^{14}C data. With the Aegean's limited area it is expected that events would be (virtually) synchronous across the basin and the occurrence of the sapropel S1 provides a useful interval with suppressed bioturbation. We use a multi-proxy approach to reduce parameter-specific bias, such as: regional asynchroneity or patchiness in faunal records; post depositional re-oxygenation of sapropel tops [Higgs et al., 1994; Thomson et al., 1995]; or more general signal disturbances by, for example, bioturbation and reworking. An event-based stratigraphy enables the assembling of dates from several cores into a "master" stratigraphic framework with the potential to assess the error in any one individual dating. This allows insight into both temporal and spatial gradients. The event stratigraphic framework may provide further studies with a means to assess chronostratigraphy in considerable detail and hence, to provide guidance for targeting new AMS radiocarbon datings.

Methods

We present results for three gravity cores on a transect through the Northern Aegean Basin (SL-11, SL-21 and SL-31), an additional gravity core (SLA-9) and two piston cores from the Southern Aegean (LC-21) and from the Levantine Sea (LC-31). All six cores consist of microfossil-rich hemipelagic ooze with a clearly defined darker band of sapropelic material. Core locations are shown in FIGURE 1, with their exact coordinates and water depths detailed in TABLE 1.

Each core was sampled in a contiguous sequence: SL-21, SL-31 and SLA-9 at 0.5cm intervals; and LC-31 and LC-21 at 1cm intervals for faunal analysis. Cores SLA-9, LC-21 and LC-31 were also sampled at 1cm intervals for geochemical analysis. The faunal samples were freeze-dried, weighed, and selected (weighed) sub-samples were disaggregated and wet sieved using demineralized water. The sieved fractions were collected on 600, 150, 125 and 63μm mesh sizes. The >150μm fractions were sub-divided using a random splitter to provide an aliquot of at least 200 individual planktonic foraminifera, providing a significance level of at least 95% for species of 4% or greater relative abundance, (see Fatela and Taborda [2002]). These were then identified, sorted on Chapman slides, and counted. Results were recorded as absolute abundance in numbers g^{-1} sediment dry weight and as relative abundance or percentages. We present here only the percentages, for brevity (FIGURE 2).

Detailed stable oxygen and carbon isotope records have been constructed for several individual planktonic foraminiferal species in cores LC-21, LC-31, SLA-9, SL-11, SL-21 and SL-31, with resolutions in the order of 1cm (FIGURE 3). The species selected were: the shallow, surface-dwelling *Globigerinoides ruber* (white); and the deep-living species *Neogloboquadrina pachyderma* (right coiling) which has been associated with the Deep Chlorophyll Maximum at the base of the euphotic layer[Rohling and Gieskes 1989, 2004; Rohling et al. 1995]. This selection follows global and specific Mediterranean habitat descriptions [Hemleben et al 1989; Pujol and Vergnaud-Grazzini 1995; De Rijk et al., 1999; Hayes et al., 1999; Rohling et al., 1993, 1995, 1997, 2004], which are corroborated for the study area by isotopic evidence [Casford et al., 2001, 2002]. The stable isotope analyses were performed at two separate inter-calibrated facilities at the National Oceanography Centre (NOC) on a Europa Geo 20-20 with individual acid bath preparation; and at NERC Isotope Geoscience Laboratory (NIGL), Keyworth on the VG-Optima with a common acid bath preparation. Isotope results are reported in ‰ deviations from the Vienna Pee Dee Belemnite standard. Analytical errors are in the order of 0.06 ‰ (1σ).

Samples for geochemical were freeze-dried, providing approximately 5g of dried material for analysis in LC-31 and 3g in SLA-9 and LC-21. Samples from cores LC-21 [see Mercone et al., 2000] and LC-31 were analysed by X-Ray Fluorescence (XRF) at NOC. The dried sample was ground in an agate mortar, then 3g was pressed into disc shaped pellets and the pellets analysed for minor elements. The remaining 2g of material was treated with a fluxing agent and melted to form glass beads that were analysed for major elements. Core SLA-9 was analyzed for concentrations of Al, S, Ba, Ca, Mn, Fe and P by Induced Coupled Plasma – Optical Emission Spectroscopy (ICP-OES). Dried, ground samples were determined from digestion in a mixture of HF, HNO_3 and $HClO_4$ and final solution in 1 M HCl. This method is adapted from Li et al [1995]. We note that the two methods can give significantly different values for certain elements, especially lithophiles, because of incomplete extraction.

Radiocarbon dates

AMS radiocarbon dates were obtained for cores LC-21, LC-31, SLA-9 and SL-31 using handpicked clean planktonic foraminiferal tests with no evidence of pyritisation or overgrowth. The samples were too small for mono-specific dating [Bard et al. 1987], but no systematic differences would be expected within the Mediterranean basin for such dates relative to clean total planktonic foraminiferal tests [cf. Jorissen et al., 1993]. The picked material was submitted for analysis at the NERC radiocarbon laboratory at SUERC (LC-21, LC-31) and at the Leibniz AMS Laboratory at Kiel (Germany) (SLA-9, SL-31). Datings for the other cores discussed here have been presented previously: cores SK-1 [Zachariasse et al., 1997], IN68-9 [Jorissen et al., 1993, Rohling et al., 1997], and C-40 [Geraga et al., 2000]. We calibrate radiocarbon ages in this paper using the IntCal Marine04 curve and the program Calib 5.1 [Stuiver and Reimer 1993, Hughen et al 2004a] with reservoir-age corrections (ΔR) as discussed in the text.

Radiocarbon datings are best seen as a direct expression of the concentration of ^{14}C (abbrv. [^{14}C]). As such, they contain three components: the age controlled reduction in [^{14}C] from original concentrations common in all cores; a reservoir age effect, which for any given time slice is likely to be very similar in the cores presented here due to their close proximity; and an undetermined contribution of old carbon, which may vary considerably between individual core samples. The radiocarbon convention ages obtained are shown in Table 2. To obtain reliable calibrated ages, an accurate assessment of the reservoir age effect and of the calibration to calendar years is needed. Both of these require fore-knowledge of the error in the undetermined old carbon contribution, with small increases in the uncertainty of uncorrected ages adding considerably to the errors in calibrated ages. Here, we present two direct date comparisons using uncalibrated ages and calibrated ages both constrained by basin-wide synchronous events. This event stratigraphy allows us to produce a reduced-error age model for uncalibrated and calibrated radiocarbon concentrations in the Eastern Mediterranean. These two approaches are complementary to one another. The uncalibrated age model makes no assumption of error size, and so provides an independent assessment of the size of the total uncertainty, but it is based on the assumption that reservoir age effects are similar between cores (see discussion). The calibrated model allows us to directly assess the component causes of uncertainty in individual samples, but requires that we make assumptions about the size of these uncertainties before calibrating the dates. Together these two approaches allow us to assess the potential errors in both the dating and calibration process.

The Event Stratigraphy

We identify and describe 24 faunal, isotopic and geochemical events and use these to define a stratigraphically controlled chronology. Each event is identified by either a sharp change in gradient with time or by alternations of presence and absence in the case of faunal changes. We divide these events into 12 primary and 12 ancillary events. The primary events are defined as occurring in all cores (analysis permitting) and appear to be basin wide. Ancillary events (mostly faunal) are defined as those that occur only in some of the cores and/or those that may have the potential to give a local or asynchronous expression.

Primary events are sub-divided into isotopic, faunal and chemical. These are detailed, together with the depth of occurrence, by core, in TABLE 3.

The 3 primary isotope events were defined as occurring at the point of inflection for the major gradient changes (see FIGURE 3). We recognize: (1) the inflection in the *N.pachyderma* $\delta^{18}O$ depletion immediately below base of the sapropel; (2) the high point at the shoulder of the $\delta^{13}C$ *G.ruber* depletion sited around the onset of the sapropel; and (3) the inflection in $\delta^{18}O$ *G.ruber*, marking the start of the depletion sited immediately below base of the sapropel (T1b). This final isotope event is similar in character to isotope event (1). However, it appears to occur earlier than the $\delta^{18}O$ *N.pachyderma* inflection. The nature and causes of these events are examined in more detail in Casford et al. [2002] and [2003].

Faunal events are identified on exits, entries and particularly strong inflections in the faunal record. Both absolute and relative abundance records were used to establish the exact levels of entries and exits. Inflections in the record were taken from relative abundance plots only and may reflect population shifts rather than changes in absolute numbers of the individual species listed. The primary faunal events (FIGURE 2 and TABLE 3) are: (4) the exit or low in *G.inflata* above peak at top of sapropel; (5) the first (near) absence of *O.universa* above the sapropel; and (6) the minimum or absence in *G.inflata* near the top of the sapropel, which is followed by a rapid increase in *G.inflata* on or shortly after the top of the darker sapropelic material. Next, we use (7) the last absence of *O.universa* before the sapropel; (8), the end of the ramping down in *T.quinqueloba* relative abundance below the sapropel, which often ramps down to zero abundance; and (9) the first, rapid increase in *G.ruber* located below the sapropel, marking the shift from very low values or absence to the higher Holocene/sapropel levels. This population shift seems to be associated with the isotopic increase in $\delta^{18}O$ *G.ruber* normally identified as Termination 1a [Casford et al 2001, 2002]. This faunal point is constrained at the last low value in *G.ruber*'s relative abundance before the increase.

Chemical signals in marine cores generally record diagenetic changes within the sediment. This is a particular problem during periods of sapropel deposition which are known to suffer oxidative 'burn down'. This study focuses on the barium signal, as while there is some potential for remobilization [Dickens, 2001], the Ba/Al ratio is widely believed to reflect precipitation associated with primary productivity or at least to record syn-depositional changes, (further discussion in Calvert [1983]; Van Os et al. [1991]; Van Os et al., [1994]; Thomson et al., [1999]; and Mercone et al., [2001]). These primary geochemical events are identified by their deviation from background values, as shown in FIGURE 4: (10) the end of Ba/Al anomaly, where it returns to background values; (11) the lowest point in the saddle in the Ba/Al anomaly within the sapropel and; (12) the start of the anomaly, where the Ba/Al ratio appears to depart from background values.

Ancillary events are identified in TABLE 4 and illustrated in FIGURES 2 and 3.

We determine the regression relationships between the depths of occurrence of the primary events in each core, to allow a direct stratigraphically controlled comparison between the cores. The details of each regression are given in TABLE 1, and we show the ± 2 standard errors (SE) interval relevant for each regression on the plots (FIGURE 1). The ancillary events are also provided in these plots as validation of the primary regression. As core LC-21 is one of the best dated and most understood records in the

Eastern Mediterranean [Hayes et al., 1999; De Rijk et al. 1999; Mercone et al., 2000, 2001; Casford et al., 2002; Rohling et al., 2002; Casford et al. 2003], we use LC-21 as the standard and we plot the occurrence depth of all events in each individual core versus their equivalent depths in LC-21.

The statistically determined multi-proxy stratigraphic framework allows the production of 'stacked' age models, using the regression equations, to project both uncalibrated and calibrated AMS ^{14}C datings from the various records (TABLE 2) onto the age-depth framework of LC-21. We already have a well-constrained chronostratigraphic framework for LC-21 from its "own" AMS ^{14}C datings (TABLE 2) and by correlation to GISP II [Rohling et al., 2002], so we can use the ages projected from other cores to assess the quality of our inter-core (radiocarbon) correlations. The 2 SE intervals constrain the uncertainty in the assigned LC-21 equivalent depths. If this projection were poor, the dates from the other Aegean cores would be unlikely to fit within the established time framework. Having thus projected all datings into LC-21, the new joint dating framework can be compared against the framework based on the datings for LC-21 proper. (FIGURE 5). We conclude that our correlation model is robust. In addition, the age-depth model for LC-21 can thus be corroborated and further detailed by the addition of the projected datings from our correlated cores.

Uncalibrated Chronology

We use the new composite Aegean time frame to examine other previously published, lower resolution records from the same region: cores SK-1 [Zachariasse et al., 1997] and C-40 [Geraga et al., 2000]. These are located close to our existing cores (FIGURE 1), provide good signal comparability with our records and allow the assumption that reservoir ages between cores are small [Reimer and McCormac, 2002] (see discussion of calibrated framework below). Any differences in the reservoir ages will be constrained within the 2 SE correlation uncertainty. The depth of each identified correlation level in these cores is listed in TABLE 3 and regressions are shown in FIGURE 6. The equations for standardizing depths to the LC-21 depth-scale are shown in TABLE 1, and these were used to calculate the LC-21 equivalent depths for the datings in cores SK-1 and C-40, reported in the source publications. FIGURE 6 shows these dates against the Aegean framework of "age versus LC-21 equivalent depth" that was presented in Figure 5.

We also examine the potential use of our method in cores from outside the Aegean Sea. Two high-resolution cores were chosen: LC-31 (Levantine/Eastern Mediterranean Sea; this study) and IN68-9 (Adriatic Sea, [Jorissen et al., 1993 and Rohling et al., 1997]). These cores were selected, as both possess multi-proxy records and AMS radiocarbon datings. The identified events are detailed in TABLE 2 and the regressions are shown in FIGURE 6 and itemized in TABLE 1. As with SK-1 and C-40, we plot these cores' AMS ^{14}C datings versus LC-21 equivalent depth (based on the regressions), in comparison with our overall Aegean framework (FIGURE 5). The result provides strong endorsement of our new correlation method and of our overall Aegean chronostratigraphic framework, hence confirming that the framework is also applicable outside the Aegean Sea.

To evaluate the usefulness of our method and the resultant Aegean (and Eastern Mediterranean) chronostratigraphic framework (FIGURE 5), a critical quantitative assessment is needed. Using our chronostratigraphic framework an age can be predicted for each depth in LC-21, and therefore via the regressions, in any of the correlated cores. We can thus predict an age for all horizons at which AMS ^{14}C datings were performed. In an ideal case the predicted and analyzed values would coincide perfectly, and a plot of one versus the other (FIGURE 7) would follow a 45° line through the origin. Since most conceivable mechanisms biasing AMS ages tend to impose shifts towards older values, we expect a proportion of the datings to fall off the isoline towards older ages (shaded area). FIGURE 7 shows an excellent overall agreement between predicted and observed ages, even in datings that are entirely independent of the time-frame used for the predictions (i.e. those in LC-31, IN68-9, C-40 and SK-1).

Using the age in radiocarbon convention years, the isoline falls within 1 SE (~120 years) of the regression through all points (FIGURE 7). Within our ability to determine, these lines appear to be identical. The framework must then approach the chronostratigraphic accuracy of the dating technique itself and the spread of datings around this line will reflect the total (analytical plus material-related) error of the individual AMS datings, including any potential variation in ΔR between sites. This suggests that the total error for AMS ^{14}C datings on this type of material is of the order of ± 240 years (2 SE) in the Eastern Mediterranean.

Calibrated framework

We can follow the same process with the calibrated datings. However, before this is possible we must have a clear understanding of the size of potential errors in this process and the value for the marine carbon reservoir age. Any direct inter-comparison of dating between cores requires radiocarbon dates to be corrected for variations in production rates of ^{14}C over time (calibration), the contribution of old carbon, and to account for the marine reservoir effect.

Unlike the uncalibrated datings we need to determine the sample uncertainty and reservoir ages directly before we can accurately calibrate the dates. To do this we need to know the size of contribution of old carbon. However until technology advances enough to allow dating on single foraminifera these measurements can only be estimated. For the cores in this study we assume bioturbation to be limited to 10cm [Casford et al., 2002] except within the periods of sapropel deposition [Rohling et al., 2002]. During sapropel deposition bioturbation appears to be reduced. Only few sapropels are truly laminated, however, so in most cases there may have been some bioturbation, and an estimate of 1cm homogenisation is used in these periods. Similarly the sampling interval (an integration of several decades to centuries) will also add to the uncertainty. These sampling uncertainties together with the analytical uncertainty are detailed in TABLE 2. A simple addition of these errors suggests the uncertainties in any one dating may be as large as 1200 years and is termed sampling uncertainty in the table. i.e.

$$\delta_{\text{sampling uncertainty}} = \sqrt{(\delta_{\text{analysis}}^2 + \delta_{\text{sample range}}^2 + \delta_{\text{bioturbation}}^2)}$$

Before calibration we also need to allow for the additional 2SE uncertainty in the correlation framework.

$$\delta_{\text{total}} = \sqrt{(\delta_{\text{sampling uncertainty}}^2 + \delta_{\text{correlation}}^2)}$$

Calibration will propagate and increase these errors. Even in LC-21 (no correlation error) the median datings from calibration have an average 2σ range of 1710 years or ± 855 years and a high of 2822 (± 1411 years). This is similar to the error size suggested by the uncalibrated ages in Jorissen et al [1993]. This suggests these age differences are real and that individual datings may be rather misleading. Fortunately we can substantially reduce these errors by constructing a time framework model that benefits from error reduction by multiple datings.

Marine reservoir effect

Before calibrating we must also assess the size of the marine reservoir effect. Foraminifera fix carbon (including ^{14}C) in the form of calcite from carbonate and bicarbonate ions in seawater. ^{14}C atoms are formed in the upper atmosphere by the addition of a neutron and loss of a proton from abundant ^{14}N (present as molecular nitrogen N_2). These ^{14}C atoms immediately start to decay back to ^{14}N (by emission of a beta particle, $^{0}\beta$). Radioactive ^{14}C reacts with oxygen to form CO_2 and is incorporated into the atmospheric carbon budget. In the oceans, only surface waters can freely exchange CO_2 and hence take up this atmospheric ^{14}C signal (Broecker and Peng 1974). As ocean waters are mixed away from the surface, ^{14}C lost by radioactive decay is not longer replaced by exchange with the atmosphere. Hence, all marine waters show an aging ^{14}C signal and the longer a water mass is removed from the surface exchange the older the radiocarbon signal (Mangerud 1972). This means that any marine (foraminiferal) calcite will show an older radiocarbon age than its true age, due to the inclusion of this old carbon (Berger et al. 1966). The amount of old carbon is controlled by the depth/region of the calcite growth, the circulation regime of this site and any life effects involved in the deposition of the calcite (Mangerud 1972). Clearly, this will vary both spatially and temporally, and a 'true' reservoir age is normally impossible to determine. In practice, estimates of this reservoir age are a combination of an averaged whole ocean reservoir age of 405 years plus a local correction termed ΔR. This local correction is based on averages of several measurements across large areas, often over whole ocean basins, with an error value quoted to account for possible spatial variability and accuracy in the measurement process (Stuiver et al 1986).

In addition, a number of closed system assumptions are normally made:

1. That there is no influx of old carbon into the basin e.g. from terrestrial/riverine sources.
2. That the sample material accurately records the age of the horizon in which it is found (ie no bioturbation or re-deposition).

This can lead to considerable inaccuracies. For example even in the highly laminated-(annually) varved sediments of the Cariaco Basin with no bioturbation and little fluvial input, foram ages show a standard deviation from the varved determined age model of 42 ^{14}C years [Hughen et al., 2004b]. Hugen et al also note potential age falsifications due to contamination in some individual samples of up to 145 years.

Within the Mediterranean, Reimer and McCormac (2002) suggest that there is statistically no difference between reservoir age results recorded in all of the basins including the Aegean basin. They suggested a local reservoir age correction (ΔR) of 58 ± 85 ^{14}C yrs B.P. for the last 6 000 years. This ΔR is based on the measurement of 4 marine shells in the Aegean, a further 4 from the wider Eastern Mediterranean, and 26 measurements in the rest of the Mediterranean Sea. They also suggest that before 6 000 years B.P. changes in deep water circulation should be taken into account, notably during the period of sapropel deposition between 6 000 and 9 000 ^{14}C years BP that is known to have been characterized by reduced deep water ventilation

[Rohling, 1994; Kallel et al., 1997; Mercone et al., 2000; Casford et al., 2003]. A single shell determination of ΔR during this period of sapropel deposition gives a ΔR value of 149 ± 30 years [Facorellis et al., 1998]. Before 9 000 years B.P. circulation in the Aegean appears to have generally been similar to the modern since ~18 000 years B.P. [Casford et al., 2002]. For ages older than 18 000 ^{14}C years B.P., ΔR is harder to model, since lower sea levels reduced the shallow shelf areas essential for deep water production but colder temperatures increased the density of the surface waters. Siani et al., (2001) attempted to resolve uncertainty prior to 12 000 years B.P. by dating planktonic foraminifera associated with marine tephras. They determined 7 values for surface water age over the last 18 000 years, 5 of which correspond to the modern values during the Holocene, Younger Dryas and the Last Glacial Maximum. The remaining 2 values at 15 700 and 17 000 years both show noticeable increases in surface water age. However this calculation assumes no bioturbation in the marine samples. Siani et al. explicitly state this assumption, justifying it by pointing to the high sedimentation rate of "~35 cm in 1 000 years". This is somewhat problematic, since such marine tephras are normally found as admixtures of marine ooze and ash and do not preclude normal bioturbation processes after deposition. Moreover when such layers comprise pure ash they do not prevent bioturbation until the time of the tephra placement. Thus even low bioturbation rates of the order of 10 cm [Casford et al., 2002] would suggest that inaccuracies in the order of 300 years remain possible. Still the arguments of Siani et al. [2001] for older surface waters in this period are both interesting and persuasive. Siani et al. also state that they cannot rule out the possibility that the two datings showing water ages older than expected, are short-lived events and constrain these excursions in ΔR to the year ranges (Siani et al., 2001). As the dates used here do not fall in either of these excursions and the bioturbation argument is not comprehensively addressed in Siani et al., [2001] we use a value for ΔR of 58 ± 85 ^{14}C yrs B.P below the sapropel (Reimer and McCormac 2002). This is consistent with Siani et al.'s five remaining datings.

Error reduction

Multi-proxy studies within the radiocarbon dating range are often supported by about 10 AMS ^{14}C datings, for reasons of economy and practicality (ie availability of material). By using these datings to construct an age model, some error reduction (relative to individual values) can be achieved. This reduction is proportional to $1/\sqrt{n}$ where n is the number of analyses. Thus, analyzing 10 samples will reduce the standard error for the framework to 31% of the average error for individual analyses. Thirty datings are required to obtain an error reduction to 18% of the total spread of data and more than 100 samples to reduce this to below 10%. Beyond 30 samples, increasing the number of datings results in only small (and decreasing) improvements in precision. We provide 30 datings inside our correlatable boundaries. This allows us to determine a calibrated age model that benefits from this error reduction. We determine that the calibrated time frame (FIGURE 5 and 6) provides an age model with uncertainties in the order of ± 350 years. Addition of more datings is unlikely to lead to substantial improvements through error reduction.

These considerations dictate that future studies in marine cores using microfossil material require at least 30 datings to constrain the chronology in systems where sediment deposition appears linear. Relating a new core to our framework would offer a cheap and easily applied tool to apply maximal error reduction for the time-stratigraphic framework of new Mediterranean cores. Every additional AMS dating correlated into our framework helps to further improve its accuracy and usefulness. We emphasize that the main effort to improve the framework is best targeted at extending the upper and especially lower boundaries of the correlated interval.

Conclusions

Material used in individual marine AMS ^{14}C datings is normally a composite of both contemporaneous and allochtonous material. This present study quantifies the total statistical error resultant from this composite. AMS dates on planktonic foraminifera or other similar material must account for the recorded variance, with the literature and the 2σ (95% of variance) results in our study suggesting the uncertainties in individual AMS datings are in the order of 1300 years.

To optimize error reductions in the chronostratigraphic of a single core, at least 30 data points are required. Our method offers a standard Eastern Mediterranean framework with 30 datings already in place, and allows optimum error reduction to the time framework of any core correlated into this framework. This framework currently gives error values of ± 240 years (2SE) for our uncalibrated time framework and ± 350 years (2σ, 95% variance) in the calibrated time framework.

Correlation of additional cores to this framework would improve these uncertainties. For correlation to the framework a strict application of the events identified here from records of multiple proxies, is required. These records should in addition rely on proxy measurements taken on same/equivalent depth samples, to ensure similar bioturbation effects etc. for all proxies in the core. The method works best if sampling resolution is better than ~200 years ensuring accurate placement of events and hence dating accuracy.

References

Bard, E., (2001) Paleoceanographic implications of the difference in deep-sea sediment mixing between large and fine particles, *Paleoceanography 16*(3), 235-239.

Bard, E., M. Arnold, P. Maurice, and J.C. Duplessy (1987). Measurements of bomb radiocarbon in the ocean by means of accelerator mass-spectrometry - technical aspects. *Nuclear Instruments & Methods in Physics Research Section B-Beam Interactions with Materials and Atoms, 29* (1-2), 297-301.

Berger, R,, R.E. Taylor, and W.F. Libby (1966) Radiocarbon content of marine shells from California and Mexican west coast. *Science 153* (3738), 864

Bethoux, J.P., B. Gentili, P. Morin, E. Nicholas, C. Pierre and D. Ruiz-Pino. (1999), The Mediterranean Sea: a miniature ocean for climatic and environmental studies and a key for climatic functioning of the North Atlantic. *Prog. Oceangr. 44*, 131-146.

Broecker, W.S. and T.H. Peng (1974) Gas-exchange rates between air and sea. *Tellus 26,* 21-35

Bromley, R. G. and N. Hanken, (2003) Structure and function of large lobed *Zoophycos* Pliocene of Rhodes, Greece. *Palaeogeography Palaeoclimatology Palaeoecology, 192*, 79-100

Calvert, S.E., 1983. Geochemistry of Pleistocene sapropels and associated sediments from the Eastern Mediterranean. *Oceanol. Acta 6*, 255–267.

Casford J.S.L., E.J. Rohling, R. Abu-Zied, S. Cooke, C. Fontanier, M. Leng, and V. Lykousis (2002), Circulation changes and nutrient concentrations in the Late Quaternary Aegean Sea: A non-steady state concept for sapropel formation *Paleoceanography 17*(2), 1-11.

Casford, J.S.L., R. Abu-Zied, E.J. Rohling, S. Cooke, K.P. Boessenkool, H. Brinkhuis, C. De Vries, G. Wefer, M. Geraga, G. Papatheodorou, I. Croudace, J. Thomson, V. Lykousis, (2001), Mediterranean climate variability during the Holocene. *Mediterranean Marine Science 2*(1) 45-56.

Casford, J.S.L., E.J. Rohling, R.H. Abu-Zied, C. Fontanier, F.J. Jorissen, M.J. Leng, G. Schmiedl and J. Thomson (2003), A dynamic concept for eastern Mediterranean circulation and oxygenation during sapropel formation. *Palaeogeography Palaeoclimatology Palaeoecology. 190,* 103-119.

De Rijk, S., E.J. Rohling and A. Hayes (1999) Onset of climatic deterioration in the eastern Mediterranean around 7 ky BP; micropalaeontological data from Mediterranean sapropel interruptions. *Mar. Geol., 153*, 337-3432.

Dickens G. R. (2001) Sulfate profiles and barium fronts in sediment on the Blake Ridge: Present and past methane fluxes through a large gas hydrate reservoir. *Geochimica et Cosmochimica Acta 65*(4), 529-543

Facorellis, Y., Y. Maniatis and B. Kromer (1998). Apparent 14C ages of marine mollusk shells from a Greek island: calculation of the marine reservoir effect in the Aegean Sea. *Radiocarbon 40*, 963-973.

Fontugne, M.R., M. Paterne, S.E. Calvert, A. Murat, F. Guichard and M. Arnold (1989) Adriatic deep water formation during the Holocene; implications for the reoxygenation of the deep Mediterranean Sea. *Paleoceanography, 4*, 199-206.

Geraga M., St. Tsaila-Monopolis, C. Ioakim, G. Papatheodorou and G. Ferentinos (2000), Evaluation of palaeoenvironmental changes during the last 18,000 years in the Myrtoon basin, SW Aegean Sea. *Palaeogeography Palaeoclimatology Palaeoecology*, *156*, 1-17.

Hayes, A., E.J. Rohling, S. De Rijk, D. Kroon and W.J. Zachariasse (1999), Mediterranean planktonic foraminifera faunas during the last glacial cycle, *Mar. Geol., 153*, 239-252.

Hemleben, C., M. Spindler and O.R. Anderson (1989) *Modern Planktonic Foraminifera* Publ. Springer, New York, 363pp.

Higgs, N.C., J. Thomson, T.R.S. Wilson, Croudace I.W.(1994) Modification and complete removal of eastern Mediterranean sapropels by postdepositional oxidation. *Geology 22* (5), 423-426.

Hughen, K.A., M.G.L.Baillie, E. Bard, A. Bayliss, J.W. Beck, C.J.H Bertrand, P.G. Blackwell, C.E. Buck, G.S. Burr, K.B. Cutler, P.E. Damon, R.L. Edwards, R.G. Fairbanks, M. Friedrich, T.P Guilderson, B. Kromer, F.G. McCormac, S.W. Manning, C. Bronk Ramsey, P.J. Reimer, R.W Reimer, S. Remmele, J.R. Southon, M. Stuiver, S. Talamo, F.W. Taylor, J. van der Plicht, and C.E. Weyhenmeyer (2004a). Marine04 Marine radiocarbon age calibration, 26 - 0 ka BP. *Radiocarbon 46*, 1059-1086

Hughen, K. A., J.R. Southon, J.H.B Chanda, B. Frantz, P. Zermeñ (2004b) Cariaco basin calibration update: revisions to calendar and 14C chronologies for core Pl07-58PC. *Radiocarbon 46* (3), 1161–1187.

Jorissen, F.J., A. Asioli, A.M. Borsetti, L.Capotondi, J.P. de Visser, F.J. Hilgen, E.J. Rohling, K. van der Borg, C. Vergnaud Grazzini, and W.J. Zachariasse (1993) Late Quaternary central Mediterranean biochronology. *Mar. Micropaleontol., 21*, 169-189.

Kallel, N., Paterne, M., Duplessy, J. C., Vergnaud-Grazzini, C., Pujol, C., Labeyrie, L., Arnold, M., Fontugne, M., and Pierre, C. (1997), Enhanced rainfall in the Mediterranean region during the last sapropel event, *Oceanologica Acta, 20*, 697-712.

Li, X., B. Coles, M. Ramsey and I. Thornton, 1995. Sequential extraction of soils for multi-element analysis by ICP-AES, *Chem Geol 124* (1–2), 109–123.

Löwemark L. and F. Werner (2001). Dating errors in high-resolution stratigraphy: a detailed X-ray radiograph and AMS-14C study of *Zoophycos* burrows. *Mar. Geol*., *177*, 191-198.

Mangerud J. 1972. Radiocarbon dating of marine shells, including a discussion of apparent age of Recent shells from Norway. *Boreas 1*, 143–72.

Mercone, D., J. Thomson, R.H. Abu-Zied, I.W. Croudace and E.J. Rohling (2001). High-resolution geochemical and micropaleontological profiling of the most recent eastern Mediterranean sapropel. *Mar. Geol. 177*, 25–44.

Mercone, D., J. Thomson, I.W. Croudace, G. Siani, M. Paterne and S. Troelstra (2000). Duration of S1, the most recent sapropel in the eastern Mediterranean Sea, as indicated by accelerated mass spectrometry radiocarbon and geochemical evidence. *Paleoceanography*, *15*, 336-347.

Pujol, A. and C. Vergnaud Grazzini (1995). Distribution patterns of live planktic foraminifera as related to regional hydrography and productive systems of the Mediterranean Sea., *Mar. Micropaleontol., 25,* 187-217.

Reimer, P J and F.G. McCormac, 2002, Marine radiocarbon reservoir corrections for the Mediterranean and Aegean Seas*, Radiocarbon 44,* 159-166.

Rohling, E.J. (1994) Review and new aspects concerning the formation of Mediterranean sapropels, *Marine Geology, 122*; 1-28.

Rohling, E.J. and W.W.C. Gieske (1989) Late Quaternary changes in Mediterranean Intermediate Water density and formation rate. *Paleoceanography, 4*, 531-545. 1989.

Rohling, E.J., F.J Jorissen, C. Vergnaud-Grazzini, and W.J. Zachariasse (1993). Northern Levantine and Adriatic Quaternary planktic foraminifera; Reconstruction of paleoenvironmental gradients. *Mar. Micropaleontol., 21*, 191-218.

Rohling, E.J., M. Den Dulk, C. Pujol, and C. Vergnaud-Grazzini (1995). Abrupt hydrographic change in the Alboran Sea (western Mediterranean) around 8000 yrs BP, *Deep-Sea Research, 42*, 1609-1619.

Rohling, E.J., F.J. Jorissen and H.C. De Stigter (1997) 200 year interruption of Holocene sapropel formation in the Adriatic Sea. *J. Micropaleontol.*, *16*, 97-108.

Rohling, E.J., M. Sprovieri, T.R. Cane, J.S.L. Casford, S. Cooke, I. Bouloubassi, K.C. Emeis, R. Schiebel, A. Hayes, F.J Jorissen, and D. Kroon, (2004) Reconstructing past planktic foraminiferal habitats using stable isotope data: a case history for Mediterranean sapropel S5, *Marine Micropaleontology, 50*, 89-123.

Rohling, E.J., P.A. Mayewski, R.H. Abu-Zied, J.S.L. Casford and A. Hayes (2002) Holocene atmosphere-ocean interactions: records from Greenland and The Aegean Sea. *Climate Dynamics, 20*, 257-267.

Sarnthein, M., Kennet, J.P., Chappell, J., Crowley, T., Curry, W., Duplessy, J.C., Grootes, P., Hendy, I., Laj, C., Negendank, J., Schulz, M., Shackleton, N.J., Voelker, A., and Zolitschka, B., (2000), Exploring late Pleistocene climate variations. *EOS 81*(51), 625-630.

Siani, G., M.E. Paterne, R. Sulpizio, A. Sbrana, M. Arnold and G. Haddad (2001). Mediterranean sea-surface radiocarbon reservoir age changes since the last glacial maximum. *Science, 294*, 1917-1920.

Stanley D.J., (1985) Mud redepositional processes as a major influence on Mediterranean margin-basin sedimentation. In *Geological Evolution of the Mediterranean Basin*, Ed. D.J.Stanley and F-C. Wezel publ. Springer-Verlag, 377-413.

Stuiver, M., G.W. Pearson, T. Braziunas (1986) Radiocarbon age calibration of marine samples back to 9000 cal yr BP. *Radiocarbon 28* (2b), 980-1021

Stuiver, M.,and P.J. Reimer (1993) Extended 14C data base and revised CALIB 3.0 14C age calibration program, *Radiocarbon 35*, 215-230.

Thomson, J., D. Mercone, G.J. de Lange and P.J.M. van Santvoort (1999). Review of recent advances in the interpretation of Eastern Mediterranean sapropel S1 from geochemical evidence. *Mar. Geol. 153*, 77–89.

Thomson, J., N.C. Higgs, T.R.S. Wilson, I.W. Croudace, G.J. De Lange, P.J.M. Van Santvoort (1995) Redistribution and geochemical behaviour of redox-sensitive elements around S1, the most recent eastern Mediterranean sapropel., *Geochim. Cosmochim. Acta*, *59*, 3487-3501.

Van Os, B.J.H., L.J. Lourens, F.J. Hilgen, G.J. De Lange and L. Beaufort (1994). The formation of Pliocene sapropels and carbonate cycles in the Mediterranean: diagenesis, dilution and productivity. *Paleoceanography 9*, 601–617.

Van Os, B.J.H., J.J. Middelburg and G.J. de Lange (1991). Possible diagenetic remobilisation of barium in sapropelic sediment from the eastern Mediterranean. *Mar. Geol. 100*, pp. 125–136.

Zachariasse, W.J., F.J. Jorissen, C. Perissoratis, E.J. Rohling and V. Tsapralis (1997) Late Quaternary Foraminiferal changes and the nature of Sapropel S1 in Skopelos Basin. *Πραχτιχά 5ου Πανελλήνιου Συμπόσιου Ωχεανογραφίας & Αλιείας,* ΤΟΜΟΣ-Ι, 391-394

TABLE 1. Location of cores and regression information.

Core	**Location**	*Depth*	**Regression coefficient (r^2)**	**No. of points**	**Equation**
LC-21	35° 40’ N 26° 35’ E	1522 m	-	-	-
SL-11	39° 06’ N 25° 48’ E	258 m	0.9835	9	y = 0.64x – 52.27
SL-21	39° 01’ N 25° 25’ E	317 m	0.9661	8	y = 0.49x – 24.53
SL-31	38° 56’ N 25° 00’ E	430 m	0.9743	9	y = 0.58x – 28.11
SLA-9	37° 31’ N 24° 33’ E	260 m	0.9809	9	y = 0.81x – 36.65
LC-31	35° 00’ N 31° 10’ E	2298 m	0.9599	10	y = 0.71x – 28.96
IN68-9	41° 48’ N 17° 55’ E	1234 m	0.9590	7	y = 0.82x – 66.96
C-40	36° 56’ N 24° 05’ E	852 m	0.9792	6	y = 0.70x – 29.43
SK-1	39° 04’ N 23° 94’ E	~1000 m	0.9837	6	y = 2.67x – 39.17

TABLE 2. Age control-points used in the present study, with true depths in the cores, and corrected depths (subtracting thickness of turbidites and ash-layers). Samples with codes starting CAM were prepared as graphite targets at the NERC radiocarbon laboratory and analysed at the Lawrence Livermore National Laboratory AMS facility. Sample codes AA were prepared at Scottish Universities Reactor Research Centre at East Kilbride and analysed at the Arizona Radiocarbon Facility. KIA sample codes indicate the Leibniz AMS Laboratory at Kiel. Radiocarbon convention ages were calibrated using marine mode of programme Calib5.1 [Stuiver and Reimer, 1993, 1998]. Cores LC-21, LC-31, SL-31, SLA-9, C-40 and SK-1 datings include a local ΔR correction of 149 ± 39 years [Facorellis et al., 1998] in the sapropel and a ΔR of 58 ± 85 years [Reimer and McCormac, 2002] outside of the sapropel, see text for further discussion. Dates in LC-21 are after [Mercone et al., 2000] and in C-40 after [Geraga et al., 2000]. Sedimentation rates are determined from the known radiocarbon dates in each core and a mean sedimentation rate is used in each core. Sample uncertainty is calculated as the sum of the uncertainties in sample range and in possible bioturbation range (see text). Total uncertainties include the sampling uncertainty, the stated AMS machine errors and the uncertainty in the correlation framework used to transpose these dates into the stacked time frame. Calibrated age range is given as the 2 sigma range after [Stuiver and Reimer, 1993, 1998] and the median probability age is also given. [Stuiver and Reimer, 1993, 1998].

True depth in core (cm)	Corrected depth (cm)	AMS lab. code	Uncorrected AMS ^{14}C age from direct dating or dated horizon (ka BP)	Sedimentation rate (cm kyr^{-1})	sample range (cm)	bioturbation uncertainty (cm)	correlation error 1SE (cm)	Sampling uncertainty (yrs)	Total uncertainty (yrs)	2σ lower cal range BP	2σ upper cal range BP	Median age (cal ^{14}C yrs BP)
LC-21												
50	50	CAMS-41314	3.35 ± 0.06	21.1	1	10	0	521	581	1946	4380	3139.5
95.5	85.5	CAMS-41313	4.29 ± 0.06	21.1	1	10	0	521	581	3146	5558	4328.5
137.75	127.75	CAMS-41311	5.59 ± 0.06	21.1	1	10	0	521	581	4780	7050	5905.5
161.5	151.5	CAMS-41315	7.48 ± 0.06	21.1	1	10	0	521	581	7630	7951	7794.5
174.25	164.25	CAMS-41312	8.12 ± 0.06	21.1	1	1	0	95	155	8266	8620	8437.5
179.5	169.5	AA-30364	9.01 ± 0.07	21.1	1	1	0	95	165	9329	9788	9530.5
209	199	AA-30365	11.77 ± 0.08	21.1	1	10	0	521	601	11885	14495	13218
252.5	242.5	CAMS-41316	14.45 ± 0.06	21.1	1	10	0	521	581	15329	18151	16752
LC-31												
28.5	28.5	CAMS-45864	3.45 ± 0.05	10.9	0.5	10	9.3	963	1867	0	6791	3468.5
60.5	60.5	CAMS-45863	6.12 ± 0.05	10.9	0.5	10	9.3	963	1867	2141	10513	6387
87.5	82.5	CAMS-45861	8.74 ± 0.05	10.9	0.5	1	9.3	138	1041	7166	11755	9303
96.5	91.5	CAMS-45862	8.50 ± 0.05	10.9	0.5	1	9.3	138	1041	6819	11301	9025
131.5	126.5	CAMS-45860	12.04 ± 0.05	10.9	0.5	10	9.3	963	1867	9251	18187	13596
247.5	242.5	CAMS-45859	32.96 ± 0.05	10.9	0.5	10	9.3	963	1867			
SL-31												
45.75	45.75	KIA9467	6.52 ± 0.05	8.6	0.5	10	6.8	1221	2062	2126	11425	6869
59.75	59.75	KIA9468	7.95 ± 0.06	8.6	0.5	1	6.8	174	1025	6388	10513	8395
78.25	78.25	KIA9469	9.33 ± 0.06	8.6	0.5	10	6.8	1221	2072	5681	15117	10252
85	85	KIA9470	9.99 ± 0.06	8.6	0.5	10	6.8	1221	2072	6438	15966	11035
120.25	120.25	KIA9471	14.65 ± 0.08	8.6	0.5	10	6.8	1221	2092	11291	20936	16394
SLA-9												
60.5	60.5	KIA9472	5.95 ± 0.05	12.5	0.5	10	7	840	1450	2932	9306	6202
71.5	71.5	KIA9473	6.45 ± 0.05	12.5	0.5	10	7	840	1450	3501	9947	6783
83.25	83.25	KIA9474	7.90 ± 0.05	12.5	0.5	1	7	120	730	6906	9805	8302.5
99.5	99.5	KIA9475	8.40 ± 0.05	12.5	0.5	1	7	120	730	7492	10367	8858
120.5	120.5	KIA9476	11.91 ± 0.07	12.5	0.5	10	7	840	1470	9788	16991	13401
C-40												
73.5	73.5	Beta-110420	6.83 ± 0.11	14.1	1	10	9.5	780	1564	5469	8783	7127
82.5	82.5	Beta-110419	7.83 ± 0.14	14.1	1	1	9.5	142	956	6612	10052	8240
131	131	Beta-110418	12.35 ± 0.16	14.1	1	10	9.5	780	1614	10396	17802	14003
SK-1												
143.5	143.5		3.81 ± 0.10	58.5	1	10	32.2	188	838	1968	5550	3732.5
284	284		6.58 ± 0.07	58.5	1	1	32.2	34	655	5627	8019	6876.5
524	524		9.64 ± 0.08	58.5	1	1	32.2	34	665	8720	12417	10509
690	690		13.43 ± 0.13	58.5	1	10	32.2	188	868	13345	17307	15291
IN68-9												
11.5	7.5	UTC-500	3.16 ± 0.12	9.5	0.5	10	14.2	1105	2720	0	8099	3578
54.5	38.5	UTC-1607	6.39 ± 0.06	9.5	0.5	1	14.2	158	1713	2753	10340	6599
157.25	81.25	UTC-501	9.28 ± 0.18	9.5	0.5	1	14.2	158	1833	6289	13816	10052
241.5	157.5	UTC-502	13.10 ± 0.20	9.5	0.5	10	14.2	1105	2800	8480	20827	14917
322.5	201.5	UTC-503	14.20 ± 0.30	9.5	0.5	10	14.2	1105	2900	9470	22018	15812
510.5	247.5	UTC-504	17.20 ± 0.30	9.5	0.5	10	14.2	1105	2900	14075	25580	19864

TABLE 3. Depth occurrence of primary events by core (in cm).

#	Primary Events		LC21 (corr.)	SL11	SL21	SL31	SLA9	LC31	IN689	C-40	SK-1
	Isotopes										
1		$\delta^{18}O$ *N.pachyderma* inflection below sapropel.	186.5	66.75	66.75	82.75	109.25	-	-	-	-
2		$\delta^{13}C$ *G.ruber* high before depletion into sapropel.	186.5	74.25	60.75	82.25	119.25	106.5	-	-	-
3		$\delta^{18}O$ *G.ruber* inflection below sapropel.	191.5	68.25	75.75	91.75	112.75	101.5	86.5	-	-
	Fauna										
4		Exit/low in *G.inflata* above sapropel.	106.5	22.25	27.25	28.75	50.25	49.5	27.5	40.0	271.0
5		Exit/low in *O.universa* above sapropel.	137.0	29.25	-	46.25	-	59.5	37.5	65.0	300.0
6		Last entrance of *G.inflata* in the top of the sapropel.	131.0	30.25	35.25	52.75	68.25	71.75	47.5	70.5	293.0
7		Exit/low in *O.universa* below sapropel.	190.5	67.25	74.75	85.25	121.75	-	71.5	102.5	486.0
8		Exit/end of *T.quinqueloba* ramp-down.	242.0	104.25	89.75	108.75	-	134.5	141.5	131.0	622.0
9		Last distinct low in *G.ruber* (T1a?)	263.0	117.25	102.25	121.75	-	172.5	149.5	160.5	648.0
	Chemistry										
10		Top of Barium anomaly.	120.5	-	-	-	60.5	60.0	-	-	-
11		Lowest point in Barium saddle.	153.0	-	-	-	82.5	84.0	-	-	-
12		Base of Barium anomaly.	188.5	-	-	-	113.5	99.0	-	-	-

Table 4. Depth occurrence of ancillary events by core (in cm). The final events listed are for reference only and were not used in the regression.

#	*Ancillary Events*	LC21 (corr.)	SL11	SL21	SL31	SLA9	LC31	IN689	C-40	SK-1
a	Peak in *G.siphonifera*.	-	22.25	26.25	30.25	-				
b	*G.bulloides* peak in sapropel.	-	29.25	34.75	47.25	71.25			73.0	304.5
c	Low before *G.bulloides* peak.	-	34.25	37.25	53.25	80.25			76.5	314.0
d	Start of *T.quinqueloba* pick-up in sapropel.	160.5		42.25	60.25	-			89.5	402.0
e	Last exit of *G.siphonifera* before sapropel.	200.5	67.25	64.75	88.25	114.25			98.5	486.0
f	Drop in warm/cold plot below sapropel	190.5		64.75	88.25	112.25			95.0	520.0
g	Last exit of *G.sacculifer* below sapropel.	195.5	66.25	67.25	80.25	128.25			102.5	565.0
h	*G.bulloides* low	-	77.25	74.25	91.25	-			120.5	543.0
i	Shoulder of drop in *N.pachyderma*.	249.0	77.25	74.75	92.5	-			120.5	571.0
j	Last absence of *G.ruber rosa* below sapropel.	195.5	78.25	74.75	91.25	-			-	543.0
k	First occurrence of *G.ruber rosa* before sapropel.	228.0	96.25	72.25	106.75	-			-	555.0
l	Mid point of initial $\delta^{18}O$ *N.pachyderma* depletion (T1a)	-	105.75	108.5	120.0	-			-	-
	Top of dark layer	131.0	30.25	35.25	46.75	73.0				
	Base of dark layer	174.5	58.75	58.5	77.5	112.25				

FIGURE 1. Core locations. Filled circles indicate cores presented in this study, open circles are core sites from the published literature (see text for references). Inset graphs show regressions of the depth occurrence (in cm down core) for primary events (filled diamonds) and ancillary events (open diamonds) detailed in this study. A 2 SE error bar is included for the x axis.

FIGURE 2. Relative abundance of selected planktonic foraminifera with depth, for cores presented in this study. Circled numbers locate occurrence of primary faunal events (detailed in TABLE 3) and circled letters show locations of ancillary events (detailed in TABLE 4). The dark bar represents the position of the visible sapropel.

FIGURE 3. Stable isotope records for cores used in this study. (for LC-21 also see [Casford et al., 2002 and Rohling et al., 2002]). Triangles record the isotopic data from *G. ruber* and the narrow line is a five point Gaussian smoothing of this data. Squares data points and the bold line indicate these same data points for *N.pachyderma*. Circled numbers indicate locations of primary isotopic events detailed in TABLE 3. The dark bar represents the position of the visible sapropel.

FIGURE 4. Concentration of barium in bulk sediment, expressed as the ratio Ba/Al, for cores in this study (also see Mercone et al., [2001] for LC-21). Circled numbers indicate primary geochemical events. (TABLE 3). The dark bar represents the position of the visible sapropel. We note that the Ba/Al ratio differs significantly between the cores; this may relate to differences in analytical techniques, local productivity, clay inputs or a combination of these.

FIGURE 5. Chronostratigraphic framework for LC-21 and all dated Aegean cores from this study. Showing radiocarbon convention ages and calibrated ages from our Aegean cores plotted versus a LC-21 equivalent depth. The narrow line indicates best fit regression for datings on LC-21 only, and the heavy line indicates the best-fit regression on our three Aegean Sea cores. For radiocarbon convention ages the vertical error bars represent the machine errors quoted for the datings (see Table 2) and horizontal error bars equate to the 2 SE from our ‘event occurrence versus depth’ regressions, projected on a LC-21 equivalent depth scale. For calibrated ages only vertical error bars are shown as all uncertianites must be estimated before calibration. The size of these bars represents the 1 sigma probability spread of the calibration, with median values for the date are shown as symbol points. In addition, we detail the second order polynomial for all Aegean datings, shown within the legend.

FIGURE 6. The extended, Eastern Mediterranean chronostratigraphic framework including the additional datings from C-40, Sk-1 LC-31 and IN68-9 against the regression for our three Aegean cores from FIGURE 5. Event occurrence regressions are included for to the right of the age correlation. With regressions of the depth occurrence (in cm down core) for primary events (filled diamonds) and ancillary events (open diamonds) and a 2 SE error bar on the x axis.

FIGURE 7. Evaluation of the overall time stratigraphic framework. Showing all AMS datings (radiocarbon convention and calibrated ages) plotted versus their equivalent predicted age from the event stratigraphy, determined from their LC-21 standardized depth and projected on our three Aegean core chronostratigraphic framework. The dotted box shows the extent of the area constrained by our depth occurrence regressions and the shaded area indicates the ‘fall’ direction expected for older datings. The heavy line indicates the ‘best fit’ linear regression for all AMS datings younger than 14 ka BP (ie those that fall within our correlatable boundaries) and the lighter weight line shows our projected 45^{o} ideal fit.

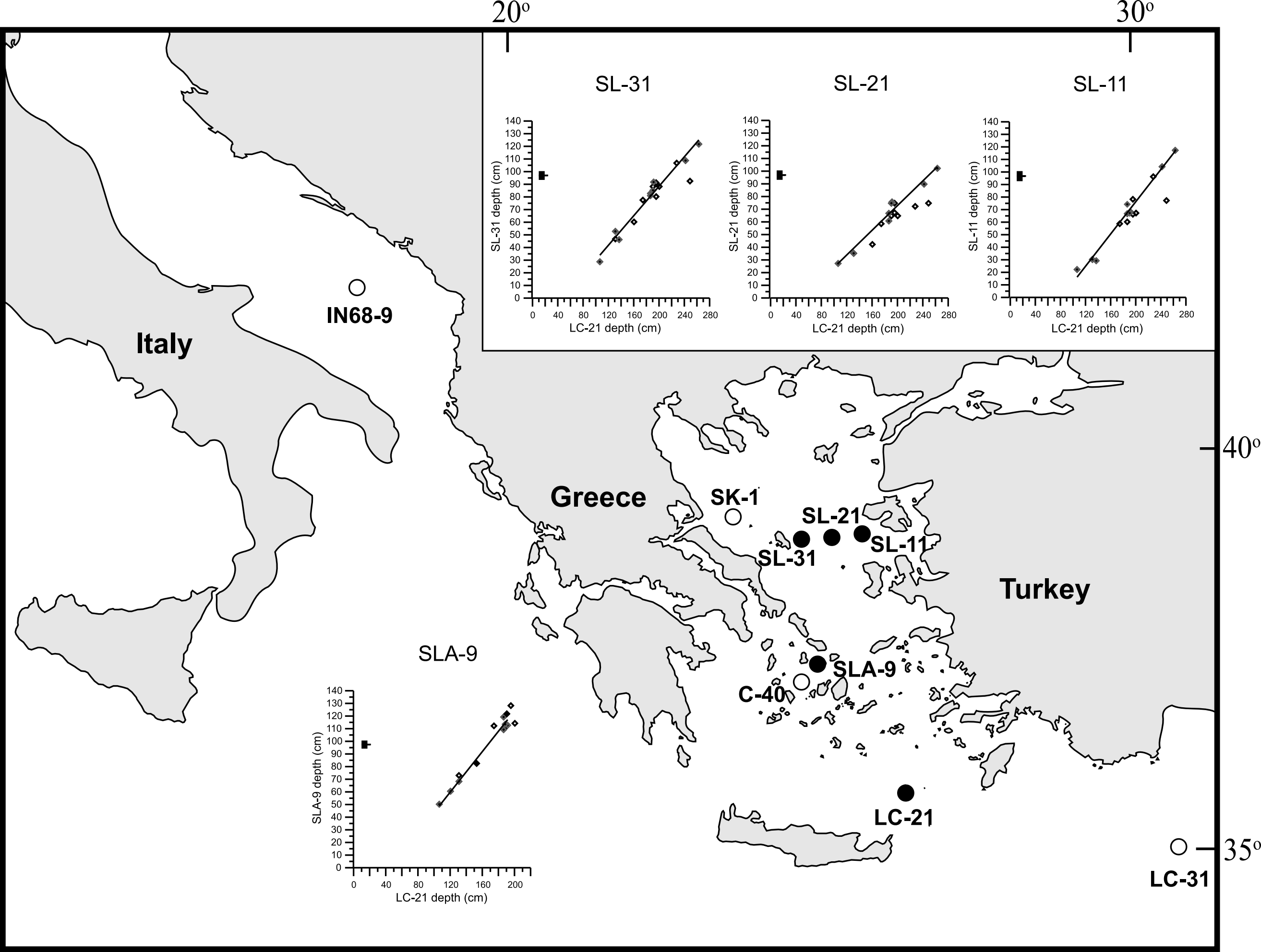
20°
30°
40°
35°
SL-31
SL-21
SL-11
SL-31 depth (cm)
SL-21 depth (cm)
SL-11 depth (cm)
LC-21 depth (cm)
LC-21 depth (cm)
LC-21 depth (cm)
IN68-9
Italy
Greece
Turkey
SK-1
SL-21
SL-31
SL-11
SLA-9
SLA-9
C-40
LC-21
LC-31
SLA-9 depth (cm)
LC-21 depth (cm)

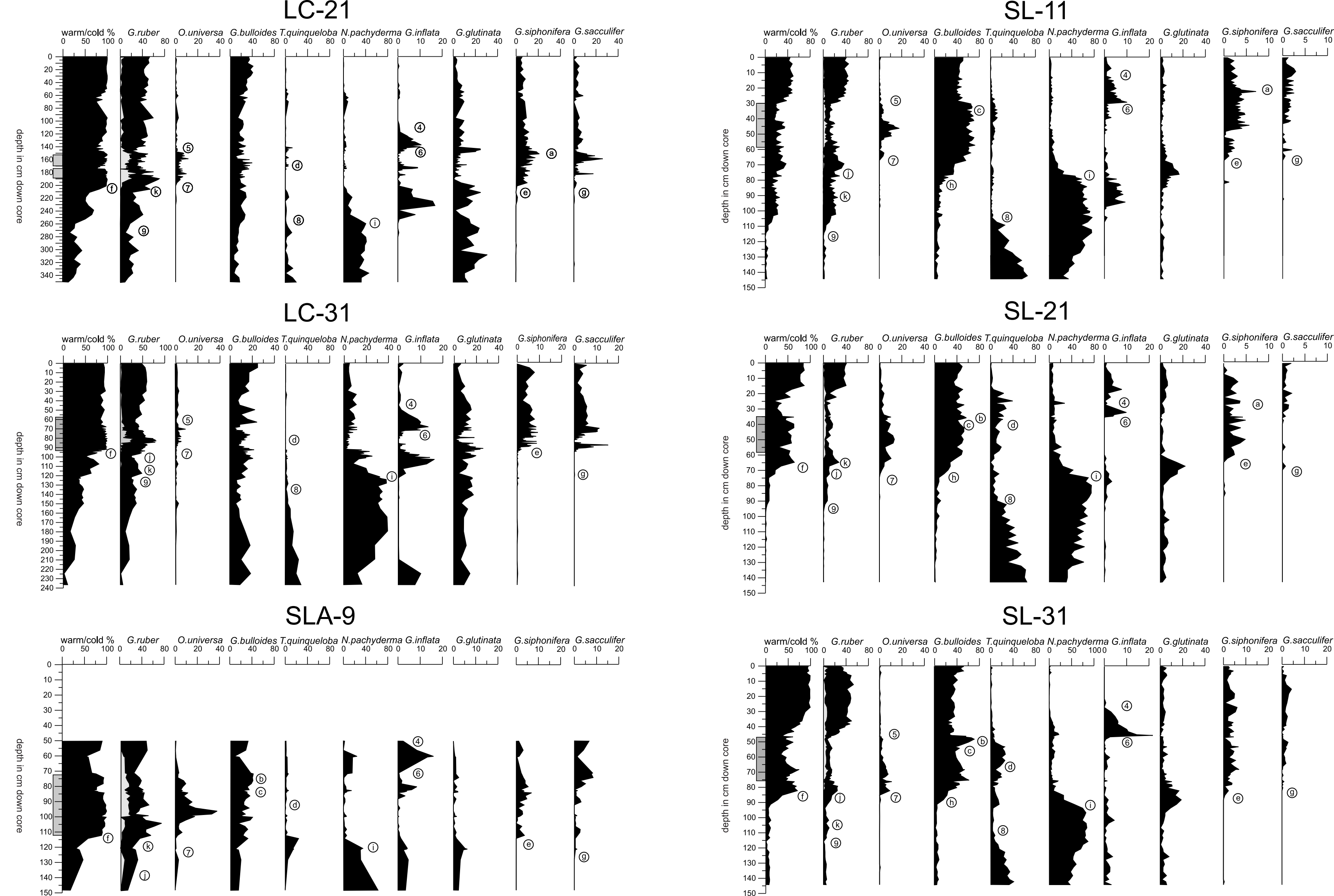

LC-21
LC-31
SLA-9
SL-11
SL-21
SL-31
warm/cold %
G.ruber
O.universa
G.bulloides
T.quinqueloba
N.pachyderma
G.inflata
G.glutinata
G.siphonifera
G.sacculifer
depth in cm down core

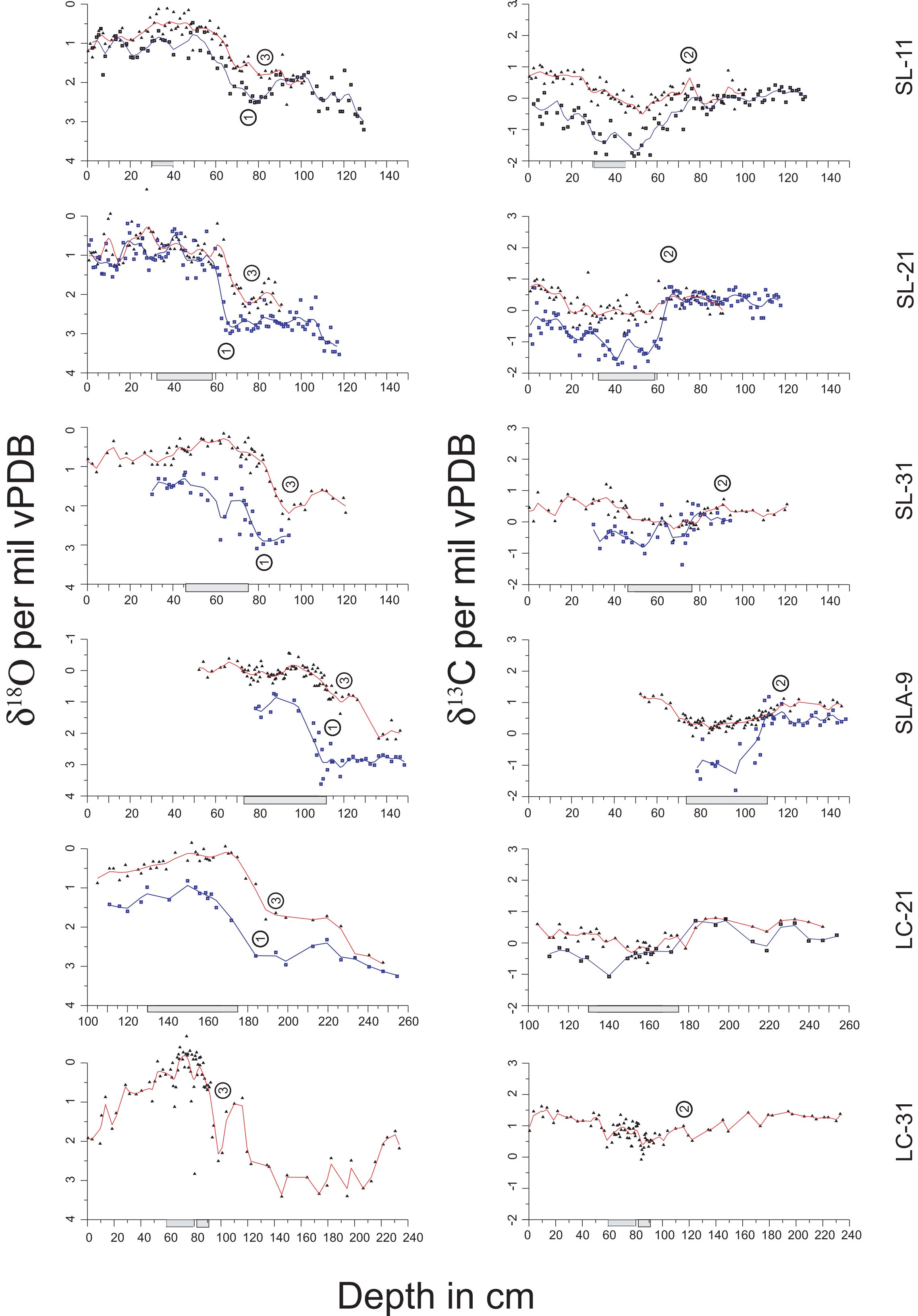

δ18O per mil vPDB
δ13C per mil vPDB
SL-11
SL-21
SL-31
SLA-9
LC-21
LC-31
Depth in cm

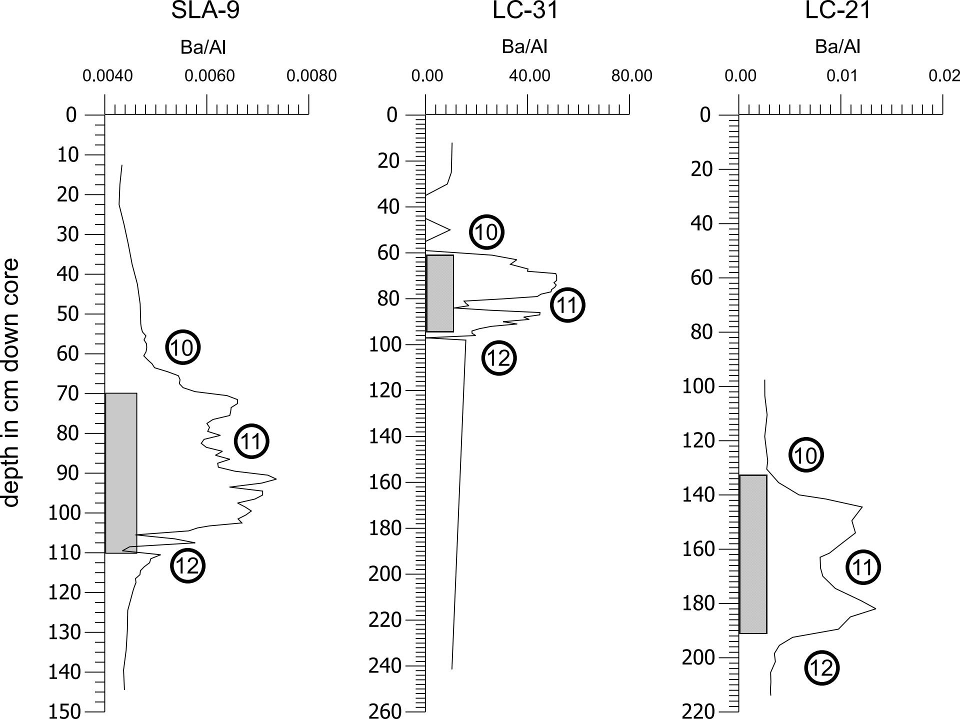
SLA-9
LC-31
LC-21
Ba/Al
Ba/Al
Ba/Al
0.0040
0.0060
0.0080
0.00
40.00
80.00
0.00
0.01
0.02
depth in cm down core
10
11
12
10
11
12
10
11
12

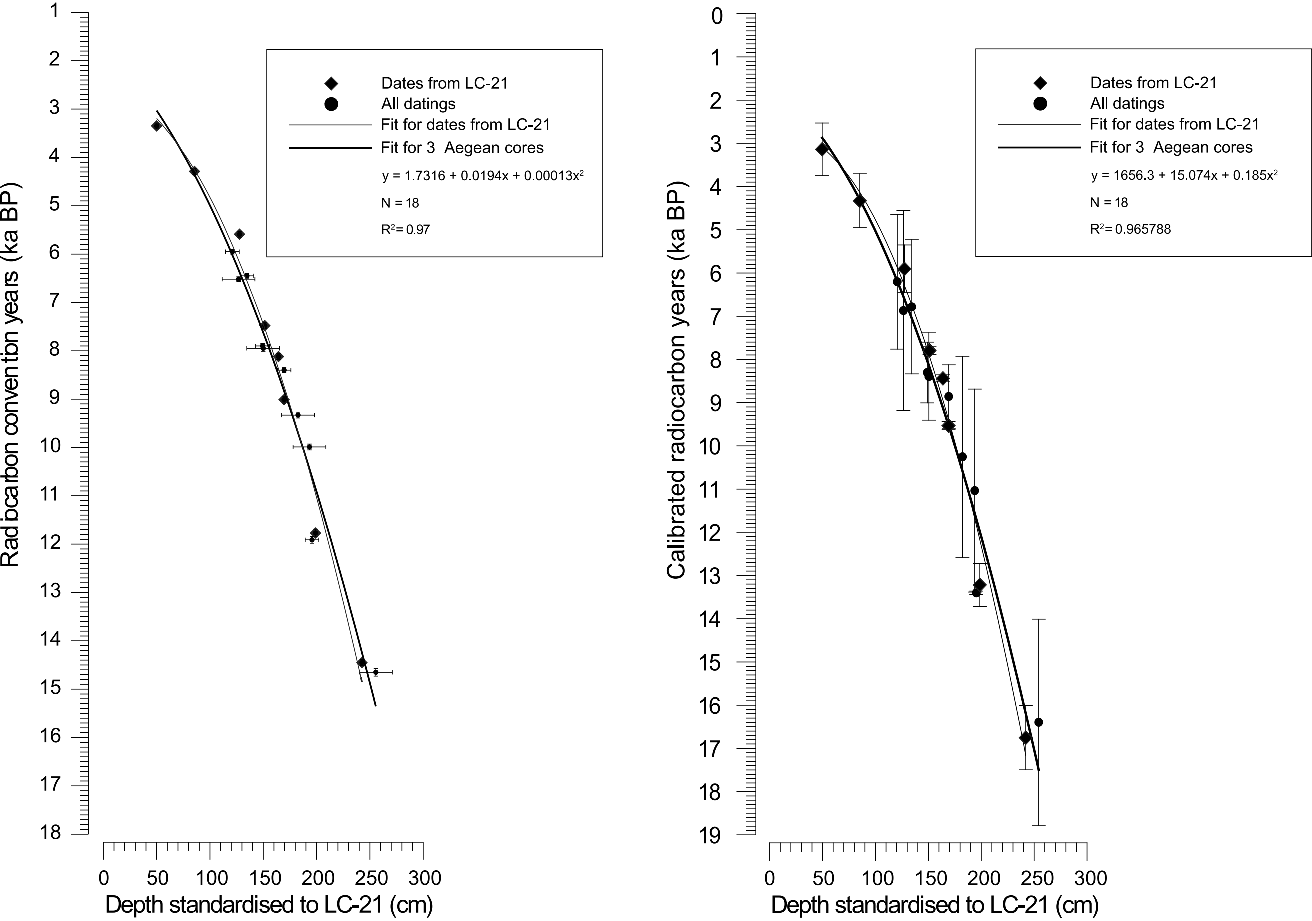
Dates from LC-21
All datings
Fit for dates from LC-21
Fit for 3 Aegean cores
y = 1.7316 + 0.0194x + 0.00013x²
N = 18
R²= 0.97
Radiocarbon convention years (ka BP)
Depth standardised to LC-21 (cm)
Dates from LC-21
All datings
Fit for dates from LC-21
Fit for 3 Aegean cores
y = 1656.3 + 15.074x + 0.185x²
N = 18
R²= 0.965788
Calibrated radiocarbon years (ka BP)
Depth standardised to LC-21 (cm)

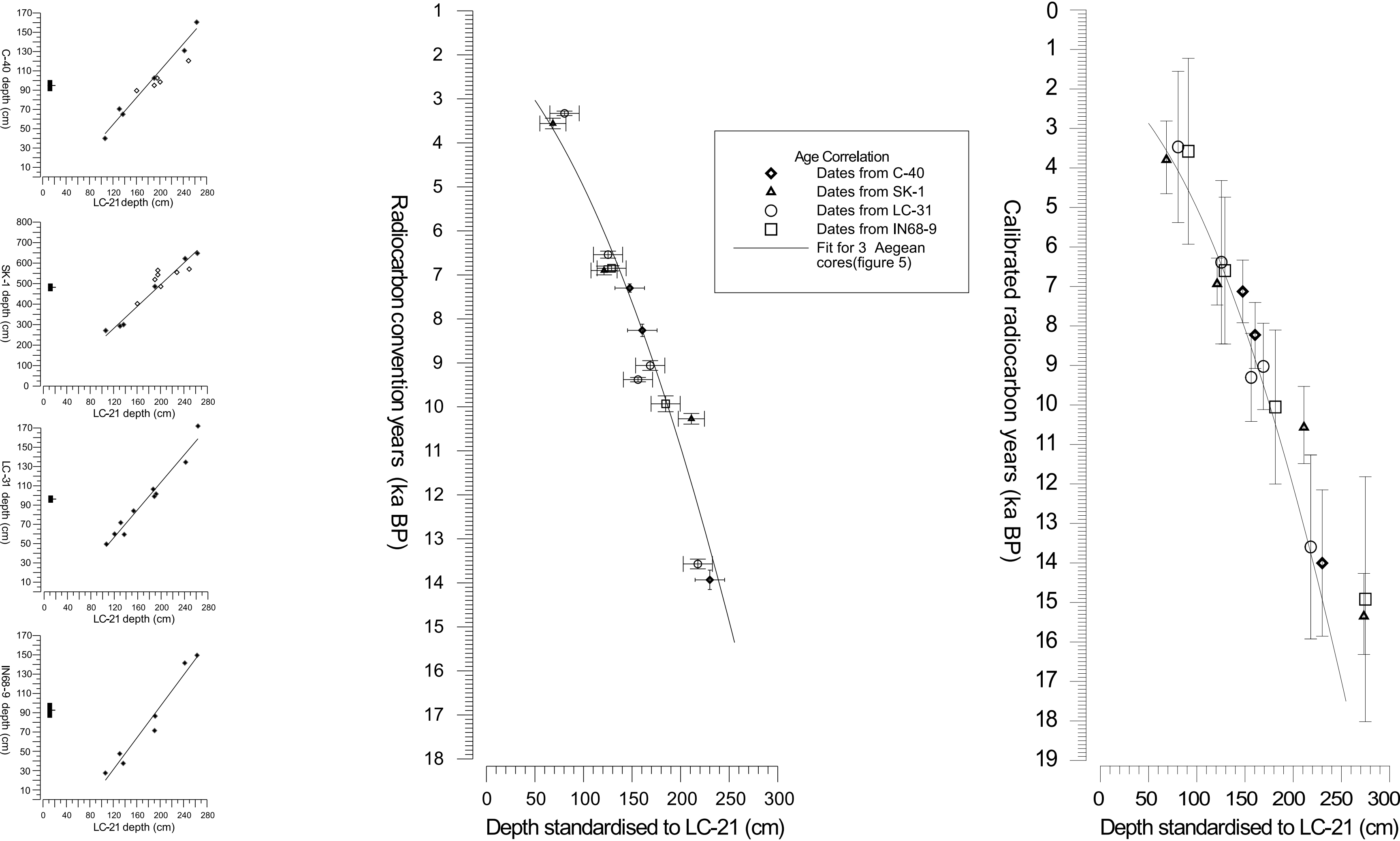
C-40 depth (cm)
SK-1 depth (cm)
LC-31 depth (cm)
IN68-9 depth (cm)
LC-21 depth (cm)
Radiocarbon convention years (ka BP)
Depth standardised to LC-21 (cm)
Age Correlation
Dates from C-40
Dates from SK-1
Dates from LC-31
Dates from IN68-9
Fit for 3 Aegean cores(figure 5)
Calibrated radiocarbon years (ka BP)

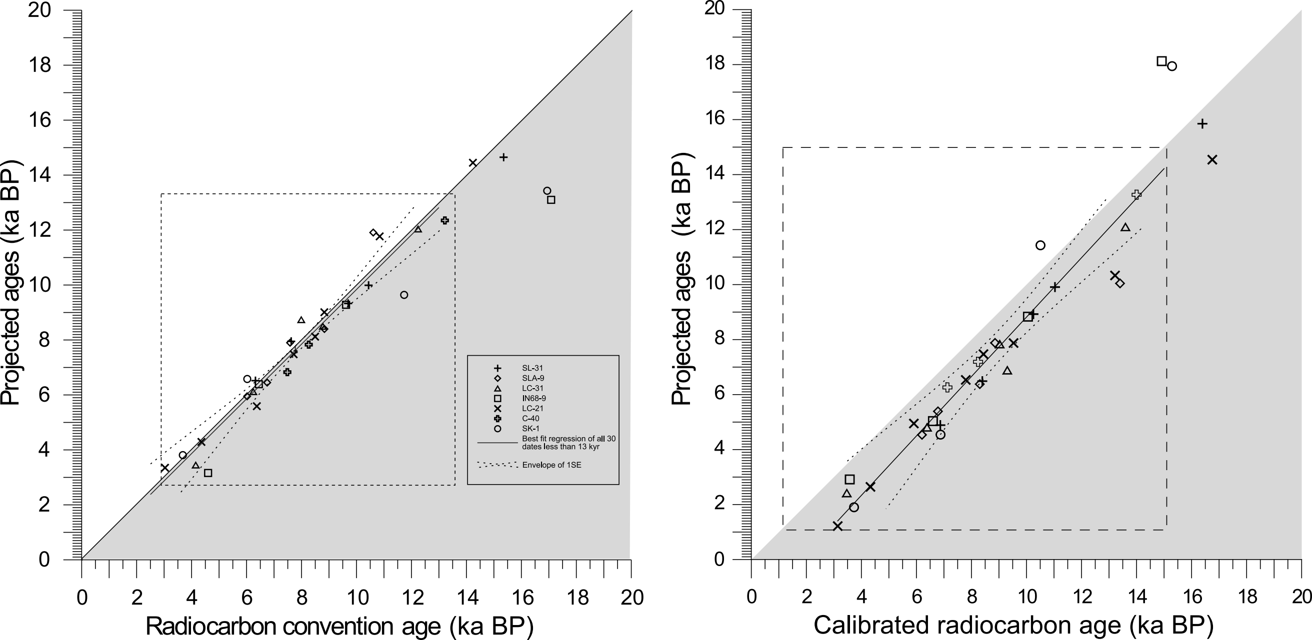
Projected ages (ka BP)
Radiocarbon convention age (ka BP)
SL-31
SLA-9
LC-31
IN68-9
LC-21
C-40
SK-1
Best fit regression of all 30 dates less than 13 kyr
Envelope of 1SE
Projected ages (ka BP)
Calibrated radiocarbon age (ka BP)